Synthetic modelling of acoustical propagation applied to seismic oceanography experiments

Jean Kormann,[1] Pedro Cobo,[1] Berta Biescas,[2] Valentí Sallarés,[2] Cord Papenberg,[3] Manuel Recuero,[4] and Ramón Carbonell[5]

Received 13 November 2009; revised 23 January 2010; accepted 12 February 2010; published 19 March 2010.

[1] Recent work shows that multichannel seismic (MCS) systems provide detailed information on the oceans' finestructure. The aim of this paper is to analyze if high order numerical algorithms are suitable to accurately model the extremely weak wavefield scattered by the oceans' finestructures. For this purpose, we generate synthetic shot records along a coincident seismic and oceanographic profile acquired across a Mediterranean salt lens in the Gulf of Cadiz. We apply a 2D finite-difference time-domain propagation model, together with second-order Complex Frequency Shifted Perfectly Matched Layers at the numerical boundaries, using as reference a realistic sound speed map with the lateral resolution of the seismic data. We show that our numerical propagator creates an acoustical image of the ocean finestructures including the salt lens that reproduces with outstanding detail the real acquired one. **Citation:** Kormann, J., P. Cobo, B. Biescas, V. Sallarés, C. Papenberg, M. Recuero, and R. Carbonell (2010), Synthetic modelling of acoustical propagation applied to seismic oceanography experiments, *Geophys. Res. Lett.*, *37*, L00D90, doi:10.1029/2009GL041763.

1. Introduction

[2] Multichannel seismic (MCS) systems, constituted by a seismic source and an array of hydrophones (i.e., a streamer), have recently been shown to be well-suited to image the ocean fine-structure with a vertical and lateral resolution of 5–10 m [e.g., *Holbrook et al.*, 2003; *Biescas et al.*, 2008]. This combined resolution is two-to-three orders of magnitude better than that of most usual hydrographic methods for horizontal direction. Seismic records provide information on the water column structure as well as hints on the oceanographic properties of the different water layers (e.g., sound speed, temperature, salinity) by processing the wavefield that is reflected at the acoustic interfaces and recorded by the streamer' hydrophones [e.g., *Sallarés et al.*, 2009; *Papenberg et al.*, 2010]. Several studies have reported reflections at these interfaces to be as weak as 10^{-4} [e.g., *Holbrook et al.*, 2003].

[3] The potential of seismic techniques as a tool to infer oceanographic properties of the ocean with high lateral resolution has sparked the interest of specialists in marine sciences other than seismologists and physical oceanographers. Underwater acousticians are concerned with the application of acoustic propagation models to seismic oceanography experiments [*Kormann et al.*, 2008], because having a precise and reliable acoustic wave propagator, well-adapted to seismic oceanography setups, is a key to further develop and apply waveform tomography schemes similar to those existing for Solid Earth [e.g., *Pratt*, 1999]. These methods could potentially allow retrieving physical properties such as water sound speed and density directly from the seismic data. However, current underwater acoustic propagation models are not optimal to be applied to seismic oceanography experiments due to two main reasons. First, underwater acoustic models threat with quasi-horizontal propagation of the acoustic wave (large distance propagation) while seismic oceanography experiments deal with quasi-vertical propagation directly beneath the system. Second, the weak reflectivity of the interfaces between water masses imposes special requirements to the numerical boundaries. As stated above, the reflection coefficients at the intra-oceanic interfaces are of order 10^{-3}–10^{-4} [e.g., *Holbrook et al.*, 2003], so the boundary conditions must guarantee a reflectivity of, at least, one order of magnitude less. This condition is virtually impossible to fulfill with classical absorbing methods, such sponge zone [*Sochacki et al.*, 1987] or classical Absorbing Boundary Conditions (ABC) [*Engquist and Majda*, 1977].

[4] An alternative is that proposed by *Kormann et al.* [2008], who combined a Finite-Difference Time-Domain (FDTD) algorithm for the propagation in the water with a first-order Perfectly Matched Layer (PML) in the boundaries based on *Berenger*'s [1994] PML model to model shot records with the precision required by seismic oceanography. The matching algorithm at the PML/medium interface was further improved by derivating a second-order PML model that ensures unconditional stability and allows the use of higher-order discretization in the space coordinates [*Kormann et al.*, 2009]. This derivation is equivalent to the Complex Frequency Shifted PML (CFS-PML) of *Roden and Gedney* [2000] but for second-order spatial convolution operator in space.

[5] In this work we use the algorithm referred to above, which combines a FDTD scheme for the propagation in the water layer with the second-order CFS-PML in the numerical boundaries, to simulate a real seismic profile acquired in the Gulf of Cadiz (SW Iberia) in the framework of the EU- "Geophysical Oceanography: A new tool to understand the thermal structure and dynamics of oceans (GO)" project.

[1]Instituto de Acústica, CSIC, Madrid, Spain.
[2]Unitat de Tecnología Marina, CSIC, Barcelona, Spain.
[3]Leibniz Institute of Marine Sciences at University of Kiel (IFM-GEOMAR), Kiel, Germany.
[4]GI2A2, Universidad Politécnica de Madrid, Madrid, Spain.
[5]Institut de Ciències de la Terra Jaume Almera, CSIC, Barcelona, Spain.

0094-8276/10/2009GL041763

Seismic and oceanographic (XBT, CTD) data were simultaneously acquired during the survey. We have used a 14 km-long sound speed model, with a lateral resolution of 6.25 m as input data to model the synthetic shot records. The high-lateral resolution reference sound speed model was constructed by inversion of MCS data acquired across a Mediterranean salt lens or Meddy [*Armi et al.*, 1989] during the GO survey, following the approach described by *Papenberg et al.* [2010]. The synthetic data were subsequently processed and stacked as with real data, to produce a synthetic record section to be compared with MCS data actually acquired along this particular line (i.e., profile GO-LR-10 of *Hobbs* [2007]).

2. Numerical Algorithm

[6] Our approach is to solve the wave equation using FDTD with high-order spatial discretization to avoid numerical dispersion. We start the derivation with the wave equation in time space-domain such that

$$\nabla^2 p - \frac{1}{c^2}\frac{\partial^2 p}{\partial t^2} + f_s = 0, \tag{1}$$

where f_s is the source function, p the pressure, and c the sound speed. A point source function will be considered and the density ρ is assumed to be constant in the water column and equal to 1032 kg/m^3, given that the contribution of density variation to water reflectivity is, in average, second order as compared to that of sound speed variation [*Sallarés et al.*, 2009]. Note that assuming constant ρ does not mean that we completely neglect, however, small density variations within the water column. Smooth changes of the mass density can be still included in the sound speed profile through the relation

$$c = \sqrt{\frac{K}{\rho}}, \tag{2}$$

where K is the compression modulus of the fluid [e.g., *Berkhout*, 1987]. Therefore, in the following we will assume that the simpler equation (1) governs the wave propagation in the physical domain. This approach has two advantages: first it saves memory and time computation, and second it makes the PML equations simpler.

[7] For the lateral absorbing boundary condition we use the PML equations proposed by *Kormann et al.* [2009], such that

$$\begin{aligned}
&-\frac{\partial \sigma_r}{\partial r}\frac{\partial q}{\partial r} + \sigma_r \frac{\partial^2 q}{\partial r^2} + \frac{\partial^2 p}{\partial r^2} - \frac{\partial^2 p_r}{c^2 \partial t^2} - \frac{3\sigma_r}{c^2}\frac{\partial p_r}{\partial t} \\
&\qquad -3\frac{\sigma_r^2}{c^2}p_r - \frac{\sigma_r^3}{c^2}q_r = 0 \qquad \text{(a)} \\
&\frac{\partial^2 p}{\partial z^2} - \frac{\partial^2 p_z}{c^2 \partial t^2} = 0 \qquad \text{(b)} \\
&q = \int_o^t p(s)ds \qquad \text{(c)} \\
&q_r = \int_o^t p_r(s)ds \qquad \text{(d)} \\
&p = p_r + p_z \qquad \text{(e)}
\end{aligned}, \tag{3}$$

where p is the pressure field, t the time, r and z are the range and depth respectively, σ_r the spatial absorbing function, and p_r, p_z, q, q_r, *and* q_z are mathematical entities without physical meaning. To integrate q and q_r in equations (3c) and (3d) we use the following finite difference scheme

$$q(t + \Delta t) = q(t)\exp(-t/t_c) + p(t)\Delta t, \tag{4}$$

where Δt is the time increment of the FDTD scheme, and t_c a stabilization parameter. The exponential factor, t_c, ensures stability for long computation times, and consequently for large scale simulation. The PML is introduced at the bottom permuting index r by z. This implies that the formulation presented in this section can be easily extended to 3D problem.

[8] A PML condition has been introduced also in the bottom, since real data do not show relevant water reflections deeper than 1800 m (i.e., the base of the Meddy). The PML zone has to ensure the reflections from the edge to be smaller than the scattered field and avoid grazing angle propagation problem [*Komatitsch and Martin*, 2007] due to the proximity of the source to the PML zone. To fulfill this requirement, we implemented a PML with a thickness of 100 times the spatial discretization. The absorbing function is a non-integrable hyperbolic one, similar to those proposed by *Bermúdez et al.* [2007]. To complete the set of boundary conditions adapted to realistic seismic oceanography setups, the pressure release $p(z = 0,r) = 0$ condition has been implemented at the surface.

3. Numerical Simulation

[9] The simulated MCS experiment reproduces the setup of the real one acquired in the Gulf of Cadiz in 2007. The section is characterized by the thermohaline intrusion at the upper part (down to 300m) and shows a prominent mesoscale feature identified as a Meddy in the depth range of 800 m to 1500 m. The model contains therefore zones, such as the core of the Meddy, where acoustic impedance contrasts and, in turn, acoustic reflectivity, should be weak; and others, such as the boundaries between neighbouring water masses, where impedance contrasts and reflectivity should be strong. The seismic source is located 8 m below the surface. The streamer is 2.4 km-long, and is composed of 192 equally-spaced (12.5 m) hydrophones, located 10 m deep.

[10] To simulate the source wavelet we have chosen a Ricker wavelet with a central frequency of 45 Hz, which is close to the central frequency of the airgun source array-used to acquire the real data. The space and time discretization are $\Delta r = \Delta z = 12.5/8 = 1.5625$ m and $\Delta t = \Delta r/1500 \approx 0.00104$ ms, respectively. A 13.125 km-long section reaching up to 1800 m-deep section has been simulated. The length of each shot-record simulation is 3.0 s, enough to cover completely the model. The stabilization parameter t_c has been set to 3000 s. The seismic line includes 233 shot records, that is, one shot every 50 m, slightly more than the 40 m spacing in the real experiment. This provides a huge gain in terms of computation time, which is the main drawback of this modelling scheme, providing at the same time an accurate reconstruction of the water column structure. It is not necessary to increase the shooting rate because stacking fold is not a relevant parameter in synthetic, noise-

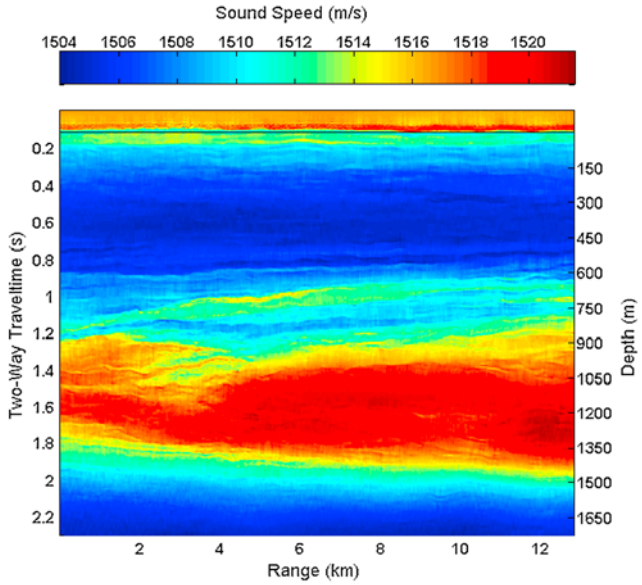

Figure 1. Inverted sound speed map (in m/s) along a section of GO-LR 10 used for modelling (modified from *Papenberg et al.* [2010]). A Meddy can be seen at depth 1000 m, crossing all the simulated section, as a strong gradient sound speed from the shallow surface zone.

free data as these ones. The wavelet propagates trough a distance between 3.6 km and 4.32 km, which implies using to use a discretization of 20 points per wavelength at less to ensure an accurate propagation and avoid numerical dispersion.

[11] The background sound speed model (see Figure 1) used to compute the synthetic seismic data along the profile has been built based on hydrographic (temperature and salinity) data recorded during the GO survey (1 XBT every 2.5 km in average along the profile) along profile GO-LR-10 [*Hobbs*, 2007]. It has been subsequently refined to the seismic resolution (1 trace every 6.25 m) using the deconvolved seismic data as a measure of the reflection coefficient field along that profile. Additional details on the inversion technique are given by *Papenberg et al.* [2010].

[12] To illustrate the adequacy of the algorithm to our problem, we present a synthetic shot-record in Figure 2. As we can observe, there are no visible reflected waves from the lateral boundaries because they are covered by the scattered field of the fine structure. We can only distinguish a weak reflection from the bottom PML with amplitude of 3×10^{-5} respect to the direct wave from time t = 2.6 s to 3.0 s (see Figure 2). It can be appreciated because it is remaining in the record due to the time propagation trough the PML zone. As it can be seen, our propagation algorithm is able to image the reflectivity at the interfaces without any blurring from the numerical boundaries. Furthermore, it allows us to discriminate the fine structure at the left edge of the Meddy. Thus, the algorithm is able to model both large and fine scale structure with the necessary level of accuracy. The main problem when simulating such complex geometry is the computational load. For the proposed model, we used a workstation with 5 cores cadenced at 2.6 GHz and 8 Go Ram. The multi-core programming allowed us to save a 40% of time computation regarding to a normal implementation with one-core computer. Nevertheless, the computation time was about 3.5 days for all the 233 shots. The main advantage is that this algorithm can be easily implemented in parallel machines and consequently increasing precision by using higher frequency central frequency for the propagated wavelet.

[13] Direct comparison between experimental and synthetic shot gathers can not be carried out due to the lower Signal to Noise Ratio of the first one. Therefore we have instead compared the experimental and synthetic stacked record sections, which correspond to the section obtained after stacking, and putting side by side all the seismic traces reflected in each common reflector point along the profile. Figure 3a shows the resulting synthetic stacked image to be compared with the experimental one (Figure 3b). We can observe the good accordance between simulated and experimental stacks. The first 0.20 s are noisy on the simulated image due to the predictive deconvolution process applied on the synthetic shot records which remove free surface ghost effects and generate some noise. From time 0.3 to 0.5 s we can observe small discontinuous reflections from the thermohaline fine structure. These events correspond quite well in both experimental and simulated images. Note that from 0.5 to 0.7 s there is an acoustic shadow zone in both images, corresponding to a zone with homogeneous water mass. From time 1.0 to 1.8 s there is a sequence of strong reflections associated to the finestructure that develops at the upper and lower boundaries of the Meddy [e.g., *Biescas et al.*, 2008]. Again the reflected events are in very good accordance: at time 0.8 s we find the main core of the Meddy, constituted by 5 dipping events. Also we can note the presence of two strong reflectors along the whole image from time 1.0 to 0.8 s. In the Meddy, there are weak reflectors at time 1.4 s and from range 6 to 12 km in both images. Finally the lower part of the experimental image do not show any reflectivity below 1.9 s, whereas in the synthetic

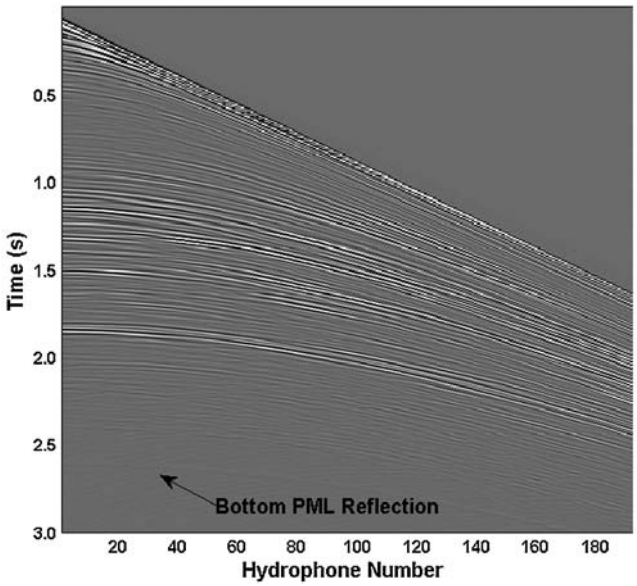

Figure 2. Synthetic shot-record of shot number 133, located at 6.650 km along the model shown in Figure 1. No spherical gain correction has been applied. Details on the acquisition system and setup are given in the text.

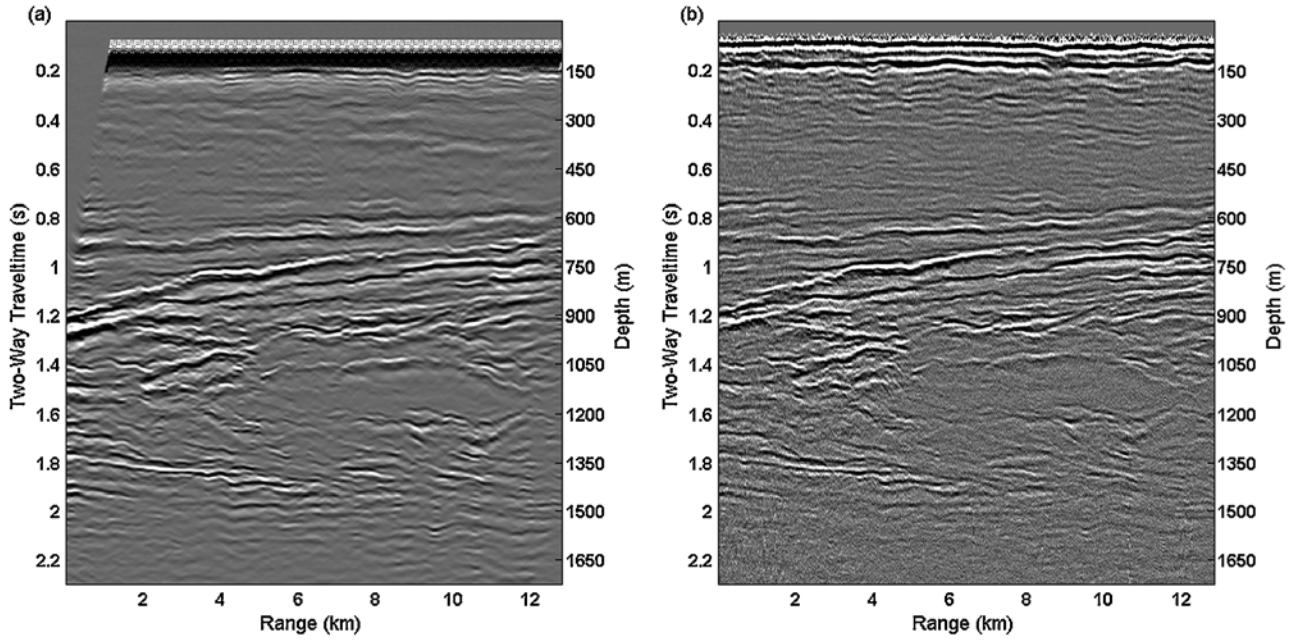

Figure 3. Comparison between (a) simulated and (b) real stacked images. The synthetic stacked image of the explored area has been obtained by using the inverted sound speed map of Figure 1 as input data. The image has been constructed by adding a total of 233 synthetic shot records.

case we can observe short, local reflectors that can not be observed in the experimental one because they are probably hidden by the ambient noise. The lowermost reflectivity is produced by weak impedance contrasts present in the local hydrographic data that give a reflectivity of the order of 10^{-5}; this is below the detectability threshold of the GO seismic system given the local ambient noise conditions.

[14] To conclude, there is a very good agreement in both time and space for the strongest reflectors. The Meddy contours are clear on both stack image and correspond well. The entire image is obtained by propagating a Ricker wavelet with central frequency equal to 45 Hz, so that the 3 dB bandwidth is ~ 20–70 Hz, and, with this wavelength we recover an image of the Meddy zone, outstandingly close to the experimental one. The great similarity between the real and synthetic data confirms that the acoustic propagator is precise and reliable enough to be used in seismic oceanography experiments. This means that it could be potentially incorporated in waveform inversion schemes to retrieve ocean sound velocity from seismic data alone, in a manner similar to what is done in Solid Earth [e.g., *Pratt*, 1999]. For real data inversion it would be preferable to use the best estimate of the actual source instead of a non-causal one as the one used here, because using a non-causal wavelet implies that the real data should have been deconvolved, which is not ideal in a full waveform inversion scheme.

4. Conclusion

[15] We have presented in this work modelling results using a FDTD algorithm for acoustic wave propagation equations that includes CFS-PML boundary conditions, applied to a seismic oceanography experimental setup. Our results show that the proposed algorithm is accurate enough to produce acoustical images of the ocean's finestructure that are almost identical to the real ones, provided we use a realistic sound speed model and a source wavelet with a bandwidth comparable to the real one. The implementation of PML is also key to mitigate the numerical edge reflections to a level below the scattered field of the water finestructure.

[16] To illustrate the efficiency of our algorithm, we have applied it to simulate a seismic oceanography survey carried out in the Gulf of Cadiz (Spain). 233 shots records were simulated, to cover a profile of ~13 km, which means one shot each 50 m. Stacked record images of both real and simulated shot records have been constructed and compared. Synthetic and real seismic sections are outstandingly similar, even if the acoustic source waveform employed in both case are not identical. The main, regional, strongest reflectors, as well as most of the shortest, weaker, local ones are well reproduced by the synthetic model. Several of the deepest and weakest interfaces are reflected in the synthetic profile but not in the real one due to ambient noise effects. We conclude therefore that our algorithm is adequate to model acoustic propagation in seismic oceanography experiments, so it could be potentially integrated in seismic waveform inversion schemes.

[17] **Acknowledgments.** The authors are grateful to Dr. Klaeschen, IFM-GEOMAR, who processed the real seismic stacked image GO-LR-10. Part of the work has been done in the framework of project MEDOC (Ref# CTM2007-66179-C02-02/MAR). Financial support from EU Spanish CSIC-founded Geocean (Ref# PIF300530F0050), FP-6 funded project GO (Ref# NEST-3003-1 Adventure FP6-015603), and MINCINN-funded TRA3008-05654-C03-03 are acknowledged.

References

Armi, L., D. Herbert, N. Oakey, J. F. Price, P. L. Richardson, H. T. Rossby, and B. Ruddick (1989), Two years in the life of a Mediterranean salt lens, *J. Phys. Oceanogr.*, *19*, 354–370, doi:10.1175/1520-0485(1989)019<0354:TYITLO>2.0.CO;2.

Berenger, J. P. (1994), A perfectly matched layer for the absorption of electromagnetic waves, *J. Comput. Phys.*, *114*, 185–200, doi:10.1006/jcph.1994.1159.

Berkhout, A. J. (1987), *Applied Seismic Wave Theory*, pp. 109–110, Elsevier, Amsterdam.

Bermúdez, A., L. Hervella-Nieto, A. Prieto, and R. Rodríguez (2007), An optimal perfectly matched layer with unbounded absorbing function for time-harmonic acoustic scattering problems, *J. Comput. Phys.*, *223*, 469–488, doi:10.1016/j.jcp.2006.09.018.

Biescas, B., V. Sallarés, J. L. Pelegrí, F. Machín, R. Carbonell, G. Buffett, J. J. Dañobeitia, and A. Calahorrano (2008), Imaging meddy fine structure using multichannel seismic data, *Geophys. Res. Lett.*, *35*, L11609, doi:10.1029/2008GL033971.

Engquist, B., and A. Majda (1977), Absorbing boundary conditions for the numerical simulation of waves, *Math. Comput.*, *31*, 629–651, doi:10.2307/2005997.

Hobbs, R. (2007), GO–Geophysical Oceanography: A new tool to understand the thermal structure and dynamics of oceans, *D318 Cruise Rep.*, Durham Univ., Durham, U. K. (Available at http://www.dur.ac.uk/eu.go/cruise/report.html

Holbrook, W. S., P. Páramo, S. Pearse, and R. W. Schmitt (2003), Thermohaline fine structure in an oceanographic front from seismic reflection profiling, *Science*, *301*, 821–824, doi:10.1126/science.1085116.

Komatitsch, D., and R. Martin (2007), An unsplit convolutional perfectly matched layer improved at grazing incidence for the seismic wave equation, *Geophysics*, *72*, SM155, doi:10.1190/1.2757586.

Kormann, J., P. Cobo, and A. Prieto (2008), Perfectly matched layers for modelling seismic oceanography experiments, *J. Sound Vibrat.*, *317*, 354–365, doi:10.1016/j.jsv.2008.03.024.

Kormann, J., P. Cobo, M. Recuero, B. Biescas, and V. Sallarés (2009), Modelling seismic oceanography experiments by using first- and second-order complex frequency shifted perfectly matched layers, *Acta Acust. Acust.*, *95*, 1104–1111, doi:10.3813/AAA.918242.

Papenberg, C., D. Klaeschen, G. Krahmann, and R. W. Hobbs (2010), Ocean temperature and salinity inverted from combined hydrographic and seismic data, *Geophys. Res. Lett.*, *37*, L04601, doi:10.1029/2009GL042115.

Pratt, G. (1999), Seismic waveform inversion in the frequency domain, part 1: Theory and verification in a physical scale model, *Geophysics*, *64*, 888–901, doi:10.1190/1.1444597.

Roden, J. A., and S. D. Gedney (2000), Convolution PML (CPML) an efficient FDTD implementation of the CFS-PML for arbitrary media, *Microwave Opt. Technol. Lett.*, *27*, 334–339, doi:10.1002/1098-2760(20001205)27:5<334::AID-MOP14>3.0.CO;2-A.

Sallarés, V., B. Biescas, G. Buffet, R. Carbonell, J. J. Dañobeitia, and J. J. Pelegrí (2009), Relative contribution of temperature and salinity to ocean acoustic reflectivity, *Geophys. Res. Lett.*, *36*, L00D06, doi:10.1029/2009GL040187.

Sochacki, J., R. Kubichek, J. George, W. R. Fletcher, and S. Smithson (1987), Absorbing boundary condition and surface waves, *Geophysics*, *52*, 60–71, doi:10.1190/1.1442241.

B. Biescas and V. Sallarés, Unitat de Tecnología Marina, CSIC, Passeig Maritim de la Barceloneta 37-49, E-08003 Barcelona, Spain.

R. Carbonell, Institut de Ciències de la Terra Jaume Almera, CSIC, C/Lluis Sole Sabaris s/n, E-08028 Barcelona, Spain.

P. Cobo and J. Kormann, Instituto de Acústica, CSIC, Serrano 144, E-28006 Madrid, Spain. (jkormann@hotmail.com)

C. Papenberg, Leibniz Institute of Marine Sciences at University of Kiel (IFM-GEOMAR), Wischhofstrasse 1-3, D-24148 Kiel, Germany.

M. Recuero, GI2A2, Universidad Politécnica de Madrid, Ctra. Valencia km 7, E-28031 Madrid, Spain.